Refraction of waves in excitable media

Leonid Pechenik and Herbert Levine
Department of Physics, University of California at San Diego, La Jolla, California 92093-0319
(Received 6 January 1998)

Waves in chemically excitable systems can refract when impinging on an interface between regions of different reaction kinetics and/or diffusion constants. Here we study this process using the thin reaction-zone limit wherein the dynamics of the system can be reduced to the tracking of the boundaries between quiescent and excited regions. We show how to derive an integrodifferential equation for the refraction of a single pulse and we subsequently solve this equation numerically. Our results predict that there can be an oscillatory recovery to the asymptotic (far from the interface) pulse; this could be checked by experiments on the Belousov-Zhabotinskii reaction. [S1063-651X(98)09309-X]

PACS number(s): 03.40.Kf

I. INTRODUCTION

There has been continuing interest in the propagation of nonlinear waves in excitable systems ranging from the Belousov-Zhabotinskii reaction [1] to cardiac tissue [2]. While many of the investigations have considered the case of a spatially uniform medium, there has been growing interest in the interaction of these waves with spatial inhomogeneities. The latter is relevant for the initiation of spiral organizing centers [3] and also for the guidance of waves in man-made structures [4].

In this work, we will study the simplest possible spatial inhomogeneity, that of a planar interface separating two regions of different reaction kinetics. This type of geometry can easily be created in the Belousov-Zhabotinskii (BZ) reaction by a variety of techniques; perhaps the simplest is the use of different illumination levels in a light-sensitive variant. There have in fact been some experiments of wave refraction in such systems [5,6], verifying, for example, that waves obey Snell's law if one measures the wave propagation directions far above and below the medium interface. One can also do direct numerical simulations of various reaction-diffusion models for this geometry [7]. Finally, a recent study by Brazhnik and Tyson [8] utilized the kinematic approximation [9] to derive the shape of the wave front. Unfortunately, in the presence of diffusion this approximation is ad hoc and cannot reliably predict the detailed response of the pulse to the presence of the interface. At the end, we will return to a discussion of our results versus those of the kinematical approach as well as versus the published experimental data.

One general approach to waves in excitable systems makes use of the usually large time-scale ratio between the slow recovery process and the excitation rise. This fact allows for the use of singular perturbation theory [10], which eventually results in the reduction of the problem to that of solving for the motion of the boundaries (wave fronts, wave backs) between excited and quiescent regions of space. This approach has been utilized for calculating the dispersion relationship for waves in the Oregonator model of the BZ reaction [11,12] as well as for their stability [13]. Also, this idea has proved quite valuable for the study of spiral waves [14–18]. Here we apply these ideas to the refraction problem.

The outline of this work is as follows. First we introduce our general modeling framework, leading eventually to a piecewise linear field equation for the recovery field with specified boundary conditions on the wave front and wave back. Specializing the refraction of a single pulse by an interface with differing kinetics, we derive an integrodifferential equation for the pulse shape. This equation can be solved far from the interface, proving Snell's law,

$$\frac{c_n^{(1)}}{\sin\,\phi_1}=\frac{c_n^{(2)}}{\sin\,\phi_2}, \tag{1}$$

for the angles made by the asymptotically straight-line fronts. We can also derive the rate of approach to these solutions, finding that the pulse in the refracting (i.e., nonincident) part of the medium can have a (decaying) oscillatory dependence on distance from the interface. Afterwards, we describe and implement a numerical procedure to fully solve the equation for one choice of parameters. Finally, we summarize our findings and point out the implications for experiments.

II. ANALYTICAL FORMULATION

We will consider a general model of a two reaction system in the form [19,20]

$$\epsilon\dot{u}=\epsilon^2 D_1\nabla^2 u+f(u,v), \tag{2}$$

$$\dot{v}=\epsilon D_2\nabla^2 v+g(u,v). \tag{3}$$

Here D_1 and D_2 are the diffusion constants for two species, u and v, and ϵ is the ratio of their reaction rates. The functions f and g have null clines of the general form indicated in Fig. 1. As discussed above, we are interested in the refraction of a pulse as it encountered a discontinuity in material parameters. This solution steadily propagates with constant velocity c along the x axis, whereas the discontinuity occurs at $y=0$. Our equations for this case will thus become

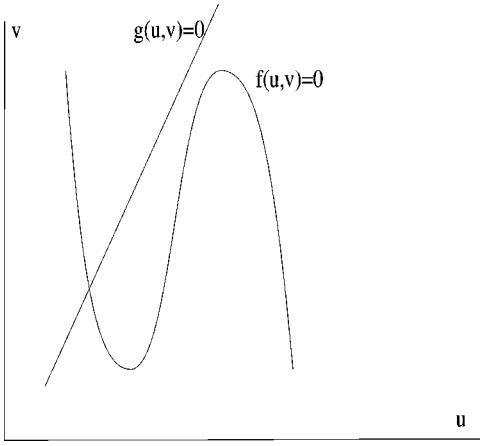

FIG. 1. Schematic drawing of the null clines for excitable medium kinetics.

$$\epsilon^2 D_1 \nabla^2 u + c\epsilon \frac{\partial u}{\partial x} + f(u,v) = 0, \tag{4}$$

$$\epsilon D_2 \nabla^2 v + c \frac{\partial v}{\partial x} + g(u,v) = 0. \tag{5}$$

It is well known [10] that these equations are decoupled in the limit of small ϵ. The equation for u in this limit yields two types of regions of slow variation in which u is algebraically related to v, separated by the regions of fast variation, which have the width of the order of ϵ^{-1}. In the slow regions u is equal to $h_+(v)$ or $h_-(v)$, the stable solutions of the equation $f(u,v)=0$; these regions are respectively referred to as excited or quiescent. In this language, a propagating pulse consists of a finite width region of excited state propagating through a quiescent medium.

To study the behavior of u and v in the transitional region it is convenient to rescale coordinates $\xi_1 = x/\epsilon$, $\xi_2 = y/\epsilon$. From the second equation of the rescaled system

$$D_1 \nabla_\xi^2 u + c \frac{\partial u}{\partial \xi_1} + f(u,v) = 0, \tag{6}$$

$$D_2 \nabla_\xi^2 v + c \frac{\partial v}{\partial \xi_1} + \epsilon g(u,v) = 0 \tag{7}$$

we find that in this region v should be equal to some constant v_0. Then, finding a suitable domain wall solution for u that goes from $h_+(v)$ as $\xi_1 \to -\infty$ to $h_-(v)$ as $\xi_1 \to \infty$ fixes the velocity as a function of v_0. The final familiar result is the eikonal relationship for the wave front,

$$c_n + \epsilon D_1 \kappa = \nu(v_f), \tag{8}$$

where $c_n = c \sin\phi$ is the normal velocity of the wave, which makes an angle ϕ with the x axis, κ is the curvature, and $\nu(v_f)$ some function of the value of the slow field at the front, v_f. This function vanishes at some specific value v^*, which is called the stall concentration. There is a similar

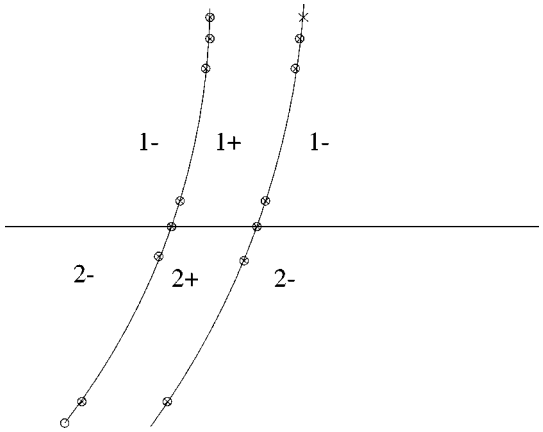

FIG. 2. Geometry and discretization for the refraction problem. The numbers refer to the two different media and +/− refers to excited/quiescent. Crosses represent positions where the coordinate is an unknown to be solved for and the circles represent places where the governing equation is evaluated.

equation for the back, which, if we use the convention that the normal vector always points into the quiescent phase, becomes

$$c_n + \epsilon D_1 \kappa = -\nu(v_b). \tag{9}$$

In the slow regions we have the equation

$$\epsilon D_2 \nabla^2 v + c \frac{\partial v}{\partial x} + g(h_\pm(v), v) = 0. \tag{10}$$

To make progress, we utilize a piecewise-linear approximation for g; this has been shown [11,12] to give quantitatively reliable results for Oregonator models of the BZ reaction, to give just one example. Specifically, we let $g(h_\pm(v),v)$ equal $\pm a_\pm - b_\pm(v - v^*)$. For convenience, we introduce a rescaling of Eq. (10):

$$c = \alpha \epsilon^{1/3} \sqrt{D_1}, \quad x = \tilde{x} \epsilon^{2/3} \sqrt{D_1},$$

$$y = \tilde{y} \epsilon^{2/3} \sqrt{D_1}, \quad (v - v^*) = w \epsilon^{1/3}. \tag{11}$$

The equation obtained in this manner is

$$\left(\frac{D_2}{D_1} \tilde{\nabla}^2 + \alpha \frac{\partial}{\partial \tilde{x}} - \tilde{b}_\pm \right) w \pm a_\pm = 0, \tag{12}$$

where $\tilde{b} \equiv b \epsilon^{1/3}$. In what follows we take $D_2 = D_1$. We furthermore use a linear approximation for the function ν, $\nu(v) = \nu'(v^*)(v - v^*) \equiv -\xi \sqrt{D_1}(v - v^*)$. This transforms the eikonal equation to

$$\alpha_n + \kappa = \mp \xi w_{f,b} \tag{13}$$

for the wave front and wave back, respectively. Here $\alpha_n = \alpha \sin\phi$.

These equations have been used as the starting point for many studies. Here, we will use this model for refraction, using the geometry shown in Fig. 2. We thus assume that we

have two different media with properties that will be labeled by the superscripts 1 and 2. To proceed, we note that the Green function of the homogeneous part of the v equation,

$$\left(\tilde{\nabla}^2+\alpha\frac{\partial}{\partial\tilde{x}}-\tilde{b}_{\pm}\right)G_{\pm}^{1,2}(\vec{r}-\vec{r}')=\delta(\vec{r}-\vec{r}') \tag{14}$$

is

$$G(\vec{r})=-\frac{1}{2\pi}K_0(A_{\pm}^{1,2}r)e^{-(\alpha/2)\tilde{x}}, \tag{15}$$

where $\vec{r}=(\tilde{x},\tilde{y})$, $r=|\vec{r}|$, $A_{\pm}^{1,2}=\sqrt{\alpha^2/4+\tilde{b}_{\pm}^{1,2}}$. The solution of Eq. (12) in every region can be written as

$$w(\vec{r})=\psi_{\pm}^{1,2}(\vec{r})\pm\frac{a_{\pm}^{1,2}}{\tilde{b}_{\pm}^{1,2}}, \tag{16}$$

where we recall that the indices $+/-$ and 1/2 label which region of space is being solved for. $\psi_{\pm}^{1,2}(\vec{r})$ are solutions of the homogeneous equations in each region, which must be determined such that the function $w(\vec{r})$ and its first derivatives are continuous everywhere. In standard fashion [21], we can relate ψ to its values on the bounding lines of each region

$$\begin{aligned}\psi_{\pm}^{1,2}(\vec{r})=\int[&G_{\pm}^{1,2}(\vec{r}-\vec{r}')\vec{\nabla}'\psi_{\pm}^{1,2}(\vec{r}')\\&-\vec{\nabla}'G_{\pm}^{1,2}(\vec{r}-\vec{r}')\psi_{\pm}^{1,2}(\vec{r}')\\&+\alpha\hat{x}G_{\pm}^{1,2}(\vec{r}-\vec{r}')\psi_{\pm}^{1,2}(\vec{r}')]\cdot\hat{n}'\,ds',\end{aligned} \tag{17}$$

where $\hat{x}$ is the unit vector in the direction of x axes, n' is outward pointing normal to the boundary, and ds' is a differential arclength. Formally, each of the ψ's can be thought of as a function in all of space, which is precisely zero when one leaves the specific region for which it is initially defined.

Let us consider for simplicity the case when the coefficients $\tilde{b}_{\pm}^{1,2}$ are the same everywhere and equal to $\tilde{b}$. We will discuss how one could treat the more general case in the Appendix. This assumption implies that the Green functions are the same everywhere. We can then greatly simplify the integrand of Eq. (17) by summing over all regions. The fact that the Green's functions are the same allows us to replace the unknown values of ψ and its normal derivative by the known discontinuities in the same quantities. After some algebra, we obtain the basic result

$$\begin{aligned}&\left((a_{-}^1+a_{+}^1)\int_{1^+\to1^-}+(a_{-}^2+a_{+}^2)\int_{2^+\to2^-}\right)\left[-\frac{\partial}{\partial n'}G(\vec{r}-\vec{r}')+\alpha\hat{x}\cdot\hat{n}'G(\vec{r}-\vec{r}')\right]ds'\\&+\left((a_{+}^1-a_{+}^2)\int_{1^+\to2^+}+(a_{-}^2-a_{-}^1)\int_{1^-\to2^-}\right)\left[-\frac{\partial}{\partial n'}G(\vec{r}-\vec{r}')\right]\Bigg|_{y'=0}dx'\pm a_{\pm}^{1,2}=\tilde{b}w(\vec{r}),\end{aligned} \tag{18}$$

where arrows under integrals show the direction of the normal $\hat{n}'$ (see Fig. 2). This form of the integral together with Eqs. (13) and (15) was used for the numerical solution of the refraction problem; this will be discussed in the next sections.

III. ASYMPTOTIC ANALYSIS

We now proceed to solve this problem numerically. In the last section, we derived an equation that must be satisfied at every point along the wave front and wave back. The only unknowns in this equation are the actual shapes of these two curves; these enter both in the arguments of the various terms in the integral as well as in the left-hand side of the eikonal equation for the field value at the fronts. Now, far from the discontinuity in the excitable media parameters, the wave fronts should be straight lines that are just the pulse solutions for the single media problems. These can be found by directly solving the field equation, leading to the expression

$$\begin{aligned}-\xi\left(\frac{a_+}{\tilde{b}}-\frac{a_++a_-}{\tilde{b}}\,\frac{A_1+A_2e^{-\lambda A_1}}{A_1+A_2}\right)&=\alpha_n,\\ \xi\left(\frac{a_+}{\tilde{b}}-\frac{a_++a_-}{\tilde{b}}\,\frac{A_2+A_1e^{-\lambda A_2}}{A_1+A_2}\right)&=\alpha_n,\end{aligned} \tag{19}$$

where λ is the width of the pulse. Note that the fact that the asymptotic pulses far above and far below the interface move at the same velocity α means that Snell's law

$$\frac{\alpha_n^{(1)}}{\sin\phi_1}=\frac{\alpha_n^{(2)}}{\sin\phi_2} \tag{20}$$

governs the angles made by these straight-line fronts.

For the numerical calculation we need to know how fast the exact solution approaches the asymptotic one. This knowledge would allow us to cut off our curve discretization at some finite point, neglecting the difference between the actual and asymptotic solutions when this difference is small enough. To proceed, we consider a small perturbation to the

plane pulse solution. The rate of decay of this (linear) perturbation to zero will govern the rate that we want to estimate (assuming it is smaller than the rate of decay of the nonlocal coupling in the governing equation; see below).

We now proceed to do the perturbative analysis directly from the field equations. The base solution of the equation (12), in a tilted system of coordinates with the y' axes along the wave back, is

$$w=\begin{cases} -\dfrac{a_-}{\tilde{b}}+\dfrac{a_++a_-}{\tilde{b}}\dfrac{A_1}{A_1+A_2}(1-e^{-A_2\lambda})e^{A_2x'} & \text{if} \quad x'<0, \\ \dfrac{a_+}{\tilde{b}}-\dfrac{a_++a_-}{\tilde{b}}\dfrac{A_1e^{A_2(x'-\lambda)}+A_2e^{-A_1x'}}{A_1+A_2} & \text{if} \quad 0<x'<\lambda, \\ -\dfrac{a_-}{\tilde{b}}-\dfrac{a_++a_-}{\tilde{b}}\dfrac{A_2}{A_1+A_2}(1-e^{A_1\lambda})e^{-A_1x'} & \text{if } x'>\lambda, \end{cases} \tag{21}$$

where $A_1=\alpha_n/2+\sqrt{\alpha_n^2/4+\tilde{b}}$, $A_2=-\alpha_n/2+\sqrt{\alpha_n^2/4+\tilde{b}}$. A small perturbation of this solution would take the form

$$\tilde{w}=\begin{cases} B_1e^{k_{x_1}x'+k_yy'}+B_2e^{k_{x_2}x'+k_yy'} & \text{in the left } (-) \text{ region}, \\ C_1e^{k_{x_1}x'+k_yy'}+C_2e^{k_{x_2}x'+k_yy'} & \text{in the right } (-) \text{ region}, \\ E_1e^{k_{x_1}x'+k_yy'}+E_2e^{k_{x_2}x'+k_yy'} & \text{in the } (+) \text{ region}. \end{cases} \tag{22}$$

There are also perturbations of the front and the back of the wave:

$$x'=\begin{cases} \delta_1e^{k_yy'} & \text{(on the back)} \\ \lambda+\delta_2e^{k_yy'} & \text{(on the front)}. \end{cases} \tag{23}$$

Solving the partial differential equation for w requires that the wave vectors obey the dispersion relation

$$k_x^2+k_y^2+\alpha_nk_x+\alpha_nk_y\cot\phi-\tilde{b}=0. \tag{24}$$

Here ϕ is the angle of the plane pulse solution and the two solutions of this equation for k_x were labeled k_{x_1} and k_{x_2} in Eq. (22).

The unknown constants in Eqs. (22) and (23) are chosen so as to satisfy boundary conditions of continuity for the function w and its first derivatives and the boundary relations (13). This leads to

$$\begin{aligned} B_1+B_2&=E_1+E_2, \\ E_1e^{k_{x_1}\lambda}+E_2e^{k_{x_2}\lambda}&=C_1e^{k_{x_1}\lambda}+C_2e^{k_{x_2}\lambda} \end{aligned} \tag{25}$$

from the continuity of w,

$$\begin{aligned} G(A_1+A_2)\delta_1+B_1k_{x_1}+B_2k_{x_2}&=E_1k_{x_1}+E_2k_{x_2}, \\ -G(A_1+A_2)\delta_2+E_1k_{x_1}e^{k_{x_1}\lambda}+E_2k_{x_2}e^{k_{x_2}\lambda}&=C_1k_{x_1}e^{k_{x_1}\lambda}+C_2k_{x_2}e^{k_{x_2}\lambda} \end{aligned} \tag{26}$$

from the continuity of the first derivatives of w, and

$$-\delta_1\alpha k_y\cot\phi-\delta_1k_y^2=\xi[B_1+B_2+G(1-e^{-A_2\lambda})\delta_1], \tag{27}$$

$$-\delta_2\alpha k_y\cot\phi-\delta_2k_y^2=-\xi[C_1e^{k_{x_1}\lambda}+C_2e^{k_{x_2}\lambda}+G(e^{-A_1\lambda}-1)\delta_2],$$

from the boundary equations. Here, $G=[(a_++a_-)/\tilde{b}]A_1A_2/(A_1+A_2)$.

These equations must be supplemented by boundary conditions at infinity. The requirement that the perturbed field vanishes far in front of the pulse leads to the condition that $\mathrm{Re}(k_{x_1}\sin\phi+k_y\cos\phi)<0$ and $C_2=0$. Behind the front, $\mathrm{Re}(k_{x_2}\sin\phi+k_y\cos\phi)>0$ and $B_1=0$. We will assume that these inequalities hold and then verify them *a posteriori* after finding the roots of k_y. This then leaves us with a homogeneous system of six linear equations with six variables. The modes are then given by demanding that the determinant be zero. The simplest way to proceed is to find B_2 and C_1 from Eq. (25) and remove them from Eq. (26); this gives

$$\begin{aligned} E_1(k_{x_1}-k_{x_2})-G(A_1+A_2)\delta_1&=0, \\ E_2e^{k_{x_2}\lambda}(k_{x_2}-k_{x_1})-G(A_1+A_2)\delta_2&=0. \end{aligned} \tag{28}$$

We then find E_1 and E_2 from Eq. (28) and remove them from Eq. (27), obtaining a system of the two linear equations:

$$\left[-k_y^2-\alpha k_y \cot\phi+G\xi\left(-\frac{A_1+A_2}{k_{x_1}-k_{x_2}}-1+e^{-A_2\lambda}\right)\right]\delta_1 + G\xi e^{-k_{x_2}\lambda}\frac{A_1+A_2}{k_{x_1}-k_{x_2}}\delta_2=0,$$
$$G\xi e^{k_{x_1}\lambda}\frac{A_1+A_2}{k_{x_1}-k_{x_2}}\delta_1+\left[-k_y^2-\alpha k_y \cot\phi + G\xi\left(-\frac{A_1+A_2}{k_{x_1}-k_{x_2}}-1+e^{-A_1\lambda}\right)\right]\delta_2=0. \tag{29}$$

Finally, we derive the relevant equation

$$\left[-k_y^2-\alpha k_y \cot\phi+G\xi\left(-\frac{A_1+A_2}{k_{x_1}-k_{x_2}}-1+e^{-A_2\lambda}\right)\right] \times\left[-k_y^2-\alpha k_y \cot\phi+G\xi\left(-\frac{A_1+A_2}{k_{x_1}-k_{x_2}}-1+e^{-A_1\lambda}\right)\right] -\left(G\xi\frac{A_1+A_2}{k_{x_1}-k_{x_2}}\right)^2 e^{(k_{x_1}-k_{x_2})\lambda}=0, \tag{30}$$

where $k_{x_1}-k_{x_2}=-2\sqrt{\alpha^2/4+\tilde{b}-k_y^2-\alpha k_y \cot\phi}$.

Once k_y is determined by the above procedure, we can estimate the distance from the interface at which we can end our discretization and use the asymptotic solution. In what follows, it is important to note that the sign of k_y plays an important part in the form of the solution. Whenever the k_y determined by solving Eq. (30) have positive real parts, the modes are allowed below the interface, but must be eliminated above the interface (where the modes do not naturally decay). The reverse is true for negative real parts. Finally, one interesting finding is that these decay constants k_y may be complex. This means that the return to the asymptotic state is not monotonic but rather is oscillatory. We will see this explicitly in our numerical solution. This represents a new prediction of our analysis.

IV. NUMERICAL METHOD

Our procedure is then to solve Eq. (13) at every discretized point. The unknowns in this equation are the x coordinates of the points, points which are equally distant along y axes with step h. The distribution of unknowns and equations are shown in Fig. 2. Below the interface, the tilt of the asymptotic line as well as the width of the pulse (and an overall constant of translation) are fixed by fixing *a priori* the coordinates of the two lower points (the one with an unfilled circle on the wave back and the point with the same y on the wave front) and all points below. Above the interface, the tilts were fixed by giving *a priori* the coordinates of all points above the final two points (with the cross on the wave front and crossed circle on the back); at these final points, we impose the equation just on the back. This then leads to a match in the number of equations versus the number of unknowns.

The remaining issue concerns the evaluation of the integrals appearing in the expression for w, Eq. (18). There are integrals over the boundaries of asymptotic solution (both above and below the medium interface), an integral along the x axis with different coefficients in the excited and quiescent regions, and finally integrals along the parts of the curves that are explicitly determined by our points. Integrals along the asymptotic lines (to infinity) were calculated numerically; since there is an exponential falloff of the integrand, this can be done to arbitrary accuracy. The integrals along the (infinitely long) parts of the x axis in the quiescent regions were transformed to an integral along all the entire x axis (which can be evaluated analytically) minus the finite integral between the boundary points of the excited region. This is then combined with the original integral over this part of the axis and evaluated numerically. Integrals along the curve passing through the points were calculated by thinking of the curves as composed of straight-line segments connecting the points. This gives an order of approximation $O(h^2)$. In the vicinity of some specific point, all finite integrals were calculated accurately using the adaptive 8-point Lagrange-Gauss algorithm. Integrals far from the point in question were calculated using a fast Simpson scheme.

Finally, we must describe how we handled the singularities in the integrand near a specific point at which we are evaluating the field. The curve of integration was divided into three regions; in the region $|x-x'|>1$, the integral (18) was evaluated numerically, as discussed above. In the region $\varepsilon<|x-x'|<1$, the integral with the singular part $(1/2\pi)\ln|x-x'|$ subtracted from the Green function was calculated numerically and the singular part was integrated analytically. In the ε vicinity of the point, the integral (18) was calculated analytically with accuracy $\varepsilon^3\ln 1/\varepsilon$. In detail, the integral $\int \vec{n}\cdot\vec{\nabla}' G\, ds'$ gives

$$\frac{1}{2\pi}\int k\, ds' + O(h^2)=\frac{\phi_2-\phi_1}{2\pi}+O(h^2), \tag{31}$$

where h is the distance between points along the y axes. Similarly, the integral of the Green's function gives

$$\frac{a_+ + a_-}{2\tilde{b}}\,\frac{\alpha\,\sin\phi}{\pi}\,\varepsilon\left(1+\ln\frac{1}{\varepsilon\sqrt{\alpha^2/4+\tilde{b}}}-\mathbf{C}+\ln 2\right) + O\left(\varepsilon^3\ln\frac{1}{\varepsilon}\right), \tag{32}$$

where $\mathbf{C}$ is Euler's constant. A remaining difficulty concerns the points that lie on the intersection of the back (or the front) with the x axis. In this pair of points, in addition to the terms already considered, a new term arises of the form $(\phi/2\pi)(a_+^1+a_-^2-a_-^1-a_+^2)/2\tilde{b}$, where ϕ is the angle between the y axis and the curve.

Our resultant system of nonlinear equations was solved by the modified Powell hybrid method. The final error of our solution (i.e., the residual) is much less than our approximation errors discussed above. In the following section, we present the results of one sample set of parameters.

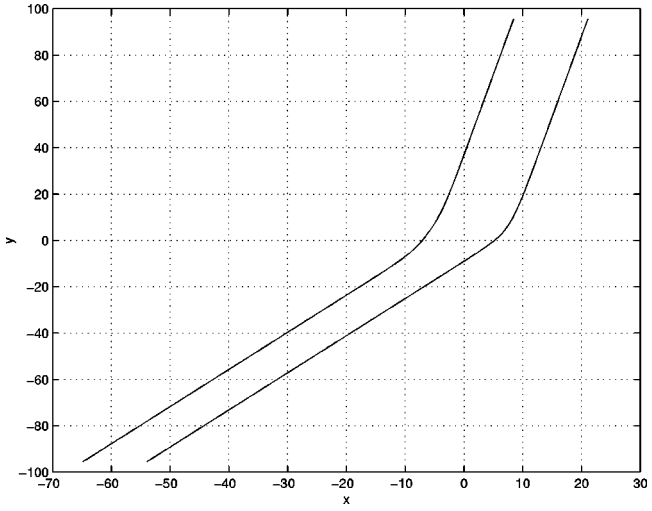

FIG. 3. Numerically determined refracted pulse shape with incident faster wave.

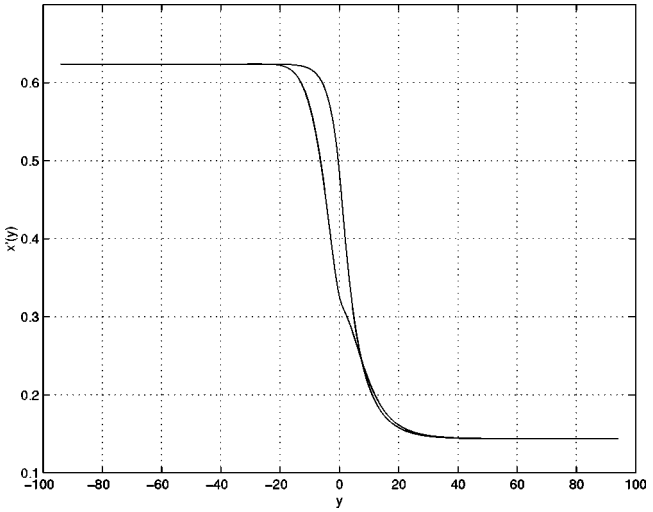

FIG. 5. Slope of the wave front and wave back vs vertical position for the case when a faster wave is incident—the wave back is the one with the wider transition region.

V. RESULTS

For our numerical calculation the following parameters were chosen: $\epsilon=0.005$, $a_+^1=0.600$, $a_-^1=0.400$, $a_+^2=0.625$, $a_-^2=0.375$, $\phi_1=\pi/2.2$, $\xi=4.0$, $b=1.0$, $D_1=D_2=1.0$. Equations (19) yield $\alpha_{n1}=1.28$, $\lambda_1=12.51$, $\alpha_{2n}=1.10$, $\lambda_2=9.25$. From Snell's law (20), $\phi_2=1.01$. The total number of equations for the problem (back and front together) was 2600. We studied two cases of refraction with a wave incident from medium 1 to medium 2 and vice versa. For the first configuration $h=0.14$ was chosen, for the second $h=0.13$.

The refraction patterns we obtained are presented in Figs. 3 and 4. In Figs. 5 and 6, we plot the slope of the wave front and wave back, showing clearly the existence of a finite-sized transition region. The transition zone spans the material boundary, with the overall effect being that the curves remain everywhere smooth. This is of course a consequence of diffusion, which disallows any sharp jumps in the wave profile.

We can compare our findings to the expected asymptotic approach rates as calculated using the formulas from the last section. For this parameter set, we determined that the slowest decaying modes had (note: we have to multiply the decay rates in y' by $\sin\phi$ to get decay rates in y) $k_y^{(a)}=-\alpha\cot\phi=-0.18$ with $\delta_2/\delta_1=1$ and $k_y^{(b)}=0.38$ with $\delta_2/\delta_1\simeq 10^{-6}$ in the first medium and $k_y^{(c)}=0.29$ with $\delta_2/\delta_1=0.07$ and $k_y^{(d)}=0.26\pm 0.16i$ with $\delta_2/\delta_1\simeq 10^{-5}$ in the second medium. Of these modes, the ones with positive (negative) real parts for k_y should appear in the approach to the asymptotic 1D pulse below (above) the material boundary.

To compare our numerical findings with this prediction, we plot in Figs. 7 and 8 the logarithm of the second derivative of our curves. In the first case studied (Fig. 7), the wave front and wave back in the upper medium show three linear (i.e., purely decaying exponential) regions; the slope in this medium is roughly $k_y^{(a)}=-0.14$ and the slope in the lower medium is $k_y^{(c)}=0.29$. These agree (to the expected level of

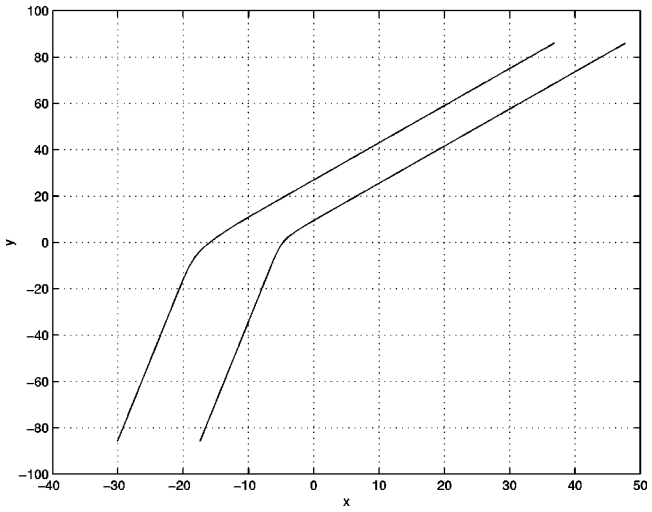

FIG. 4. Numerically determined refracted pulse shape with incident slower wave.

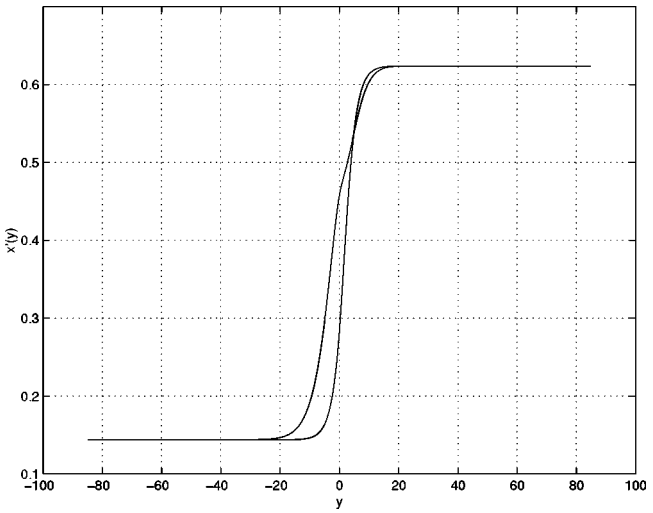

FIG. 6. Slope of the wave front and wave back vs vertical position for the case when a slower wave is incident—the wave back is the one with the wider transition region.

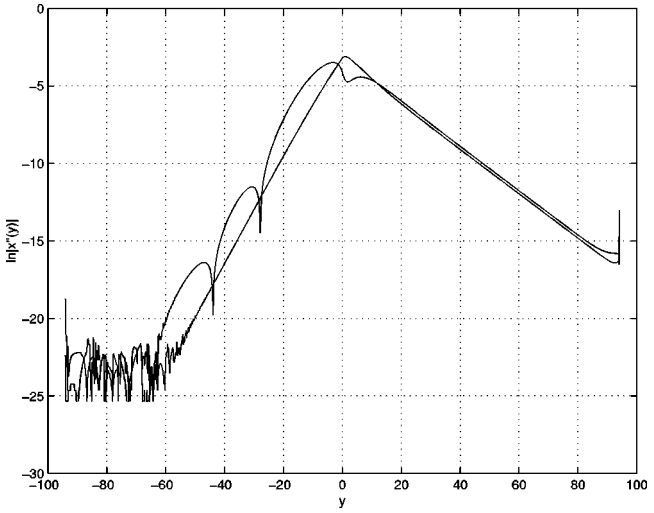

FIG. 7. Logarithm of the second derivative of the wave back (oscillatory) and wave front (nonoscillatory) curves when the faster wave is incident. The small fluctuations at the left end represent our solution accuracy; the jump at the right end is due to the residual effect of truncating to a finite discretization domain.

accuracy) with the aforementioned predictions. The wave back in the bottom medium shows an oscillatory recovery; these data are consistent with the mode $k_y^{(d)}=0.26\pm 0.16i$. The reason that this mode does not show up on the wave front is that the eigenvector for this mode has $\delta_1/\delta_2 \simeq 10^{-5}$. One can show that this ratio would be precisely zero for the diffusionless limit and hence can be estimated to be $e^{-\lambda}$ (recall that we have taken units with $D_1=D_2=1$); this explains its small size and hence the dominance of the next-to-leading mode for the wave front.

In the second case (Fig. 8) the wave front and wave back show only decaying regions. The slope for the wave back in the lower medium is consistent with the mode $k_y^{(b)}$. Finally, the wave front in both media as well as the wave back in the upper medium fall at the same rate. This rate is not given by

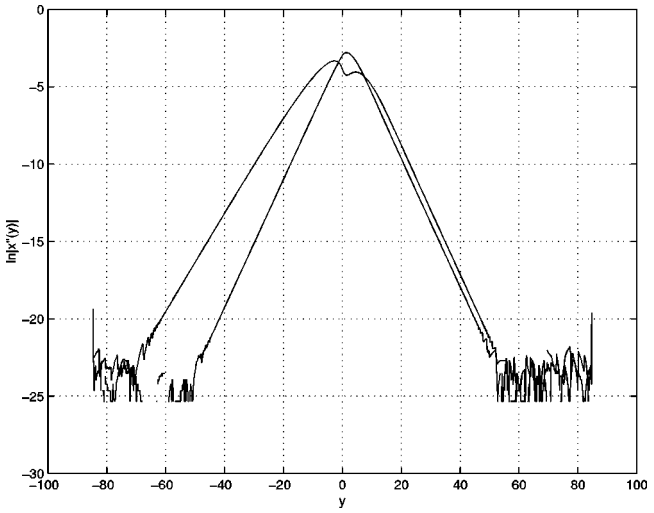

FIG. 8. Logarithm of the second derivative of the wave back (wider curve) and wave front (more narrow) when a slower wave is incident. The small fluctuations at the left and right ends represent our solution accuracy.

any modal calculation (the lowest available mode has a significantly higher falloff) but instead arises directly via nonlocal terms in the governing equation. The smallest such nonlocal term is due to the contribution to the field of the integral along the x axis; this falls off as $e^{-\sqrt{b}y}=e^{-0.41y}$. This rate agrees with our data.

VI. DISCUSSION

In summary, we have carried out a numerical solution of the pulse shape for the refraction scenario. We have shown how one can derive an exact equation for this shape and thereafter solve for it iteratively. One surprise is that the return to the asymptotic pulse can occur in an oscillatory manner, as we have seen explicitly for one of the two cases studied.

Inasmuch as nonlocality is a key ingredient in determining the actual shape, one cannot reliably use anything like the kinematic approach if one desires accurate results. The kinematic approach makes the assumption that curvature is the only contribution to changing the wave speed inside a specific medium (i.e., not on the material interface). When there is a sharp material discontinuity, however, the slow variable concentration field will not equal the respective fixed point values unless we are sufficiently far from the material interface; near the interface, diffusion will lead to a chemical field inhomogeneity and this will directly affect the propagation speed via the eikonal equation. That this must be the case can be seen by recognizing that the finite diffusion system cannot support the curvature discontinuity found in the kinematic construction. And, since the kinematic methodology has nothing at all to say about the width of the pulse, it certainly cannot predict the width oscillations that emerge from the exact solution.

As already mentioned, there has been one experiment [5] on wave refraction for the BZ system. Our calculations are in qualitative agreement with the (low resolution) published photo, but it is hard to say much more at present. The oscillatory effect will be difficult to detect by looking directly at the interface (without, say, trying to compute higher derivatives such as the curvature), and hence higher resolution studies will be needed to look for this predicted phenomenon.

Finally, our calculation with parameters chosen somewhat arbitrarily should be thought of as a proof of principle. One could carry out a similar (albeit technically more difficult calculation) for the piecewise linear reduction of the Oregonator model so as to generate more quantitative predictions for a BZ system. Although this has not yet been done, our results regarding the structure of the answer will continue to be valid for this case as well.

APPENDIX

In the text, we derived the basic equation (17) relating the field to its values and its normal derivatives along the various boundaries separating the different regions of our space. For the case of identical $b_{\pm}^{1,2}$, the equation simplified to the point where one could directly obtain the field w at the wave front and wave back in terms of known functions integrated over an unknown set of curves. This formulation was the basis of

our numerical scheme for iteratively determining the wave front and wave back shapes near the medium interface.

In the more general case, we must utilize Eq. (17) directly. Given a set of curves, the values of the functions $\psi_{\pm}^{1,2}(\vec{r})$ along the front and back are known, since

$$w(\vec{r}) = \psi_{\pm}^{1,2}(\vec{r}) \pm \frac{a_{\pm}^{1,2}}{\tilde{b}_{\pm}^{1,2}} \tag{A1}$$

and w obeys the eikonal equation. We define the normal derivative along the wave front as $\phi_f(s) = \hat{n}_+ \cdot \vec{\nabla}\psi_+ = -\hat{n}_- \cdot \vec{\nabla}\psi_-$, where the normal vectors by definition point out of the domain and we have used the continuity of the normal derivative of w across the boundary; this equation holds in both media (1 and 2). There is another similar definition for the wave back function $\phi_b(s)$. So, there is an effective doubling of the number of variables since now we must determine not only the shape of the curves but also the auxiliary field ϕ for the pulse boundaries. To match this doubling, we must have twice as many equations, that is, two per point along the curve. These are just Eq. (17) evaluated infinitesimally close to the two sides of the curve. The equation on either side alone can be thought of as determining ϕ via solving the Dirichlet problem for the field ψ in the given region; requiring that the same function ϕ determines the normal derivative of the field for the other side of the boundary is then a nontrivial condition for the curve itself. Note that the solution constructed in this manner automatically satisfies the condition that the derivative of w is continuous as we cross the pulse boundary.

Finally, we discuss what happens at the media interface. Here, not only is the normal derivative unknown, but the field value itself is unknown as well. However, the ''curve'' is now fixed to be the x-axis line. Hence the two unknowns per point can be determined by same strategy of evaluating Eq. (17) on opposite sides of the boundary. Far enough away from the pulse, the field approaches the fixed point value and hence $\psi \to 0$; this means that again one will have to treat as variables only a finite number of field and normal derivative values, as determined by the discretization size as compared to the scale over which the field relaxes.

[1] G. S. Skinner and H. L. Swinney, Physica D **48**, 1 (1990); T. Plesser, S. C. Muller, and B. Hess, J. Phys. Chem. **94**, 7501 (1990).

[2] A. Karma, Phys. Rev. Lett. **71**, 1103 (1993); R. Aliev and A. V. Panfilov, J. Theor. Biol. **181**, 33 (1996).

[3] H. Levine, I. Aranson, L. Tsimring, and T. V. Truong, Proc. Natl. Acad. Sci. USA **93**, 6382 (1996); J. Lauzeral, J. Halloy, and A. Goldbeter, *ibid.* **94**, 9153 (1997).

[4] O. Steinbock, A. Toth, and K. Showalter, Science **267**, 868 (1995).

[5] A. M. Zhabotinsky, M. D. Eager, and I. R. Epstein, Phys. Rev. Lett. **71**, 1526 (1993).

[6] O. Steinbock, V. S. Zykov, and S. C. Muller, Phys. Rev. E **48**, 3295 (1993).

[7] For a simulation of a closely related geometry, see J. Kosek and M. Marek, Phys. Rev. Lett. **74**, 2134 (1995).

[8] P. K. Brazhnik and J. Tyson, Phys. Rev. E **54**, 1958 (1996); see also Physica D **102**, 300 (1997).

[9] A. Mikhailov, V. A. Davydov, and V. S. Zykov, Physica D **70**, 1 (1994).

[10] J. J. Tyson and J. P. Keener, Physica D **32**, 327 (1988).

[11] J. D. Dockery, J. P. Keener, and J. J. Tyson, Physica D **30**, 177 (1988).

[12] D. A. Kessler and H. Levine, Physica D **39**, 1 (1989).

[13] D. A. Kessler and H. Levine, Phys. Rev. A **41**, 5418 (1990).

[14] P. Pelce and J. Sun, Physica D **48**, 353 (1991).

[15] D. Kessler and R. Kupferman, Physica D **97**, 509 (1996).

[16] D. Kessler and R. Kupferman, Physica D **105**, 207 (1997).

[17] I. Mitkov, I. Aranson, and D. Kessler, Phys. Rev. E **54**, 6065 (1996).

[18] V. Hakim and A. Karma, Phys. Rev. Lett. **79**, 665 (1997).

[19] E. Meron, Phys. Rep. **218**, 1 (1992).

[20] A. T. Winfree, Chaos **1**, 303 (1991).

[21] D. Kessler and H. Levine, Physica D **49**, 90 (1991).